Impact of Metal Clusters on the Lewis Acidity of Oxide Surfaces: First Principles Calculations of Pt_{10}/γ -Al₂O₃(110)

George Yan¹, Dionisios G. Vlachos^{1,2*}

Abstract

While the impact of the support on dispersed metal catalysts has been studied intensively, less is known about the role of the metal on the active sites of the support. Here, we investigate such "inverse" effects by assessing the interfacial acidity of Pt_{10}/γ - $Al_2O_3(110)$ through first-principles calculations, using pyridine adsorption on Al sites and H_2 dissociation over Al/O pairs as proxies for Lewis acidity. We found that Pt-Al bonding generally weakens the monodentate pyridine adsorption mode at interfacial Al sites, but interfacial metal-acid pairs enable a strongly adsorbing multidentate configuration with very different vibrational signatures. Despite a seemingly weakened Lewis acidity, some interfacial Al/O pairs are highly active for H_2 dissociation due to the divergent impact of the Pt_{10} cluster and surface reconstruction on the multiple Pt_{10} dissociation channels. The chemically diverse Pt_{10} dissociation pathways and structural perturbations of the support by the metal make traditional scaling relations inadequate. Instead, we propose site-specific transition state scaling relations to describe interfacial Pt_{10} dissociation barriers, and ultimately, to understand the influence of dispersed metal clusters on their support.

Keywords

Metal-support interactions, interfacial chemistry, surface acidity, H₂ activation, scaling relations

¹ Delaware Energy Institute, University of Delaware, 221 Academy St, Newark, DE 19716, United States

² Department of Chemical and Biomolecular Engineering, University of Delaware, 150 Academy St, Newark, DE 19716, United States

^{*} To whom correspondence should be addressed. Email: vlachos@udel.edu

1. Introduction

Dispersed metal catalysts are among the most important materials for producing commodity chemicals.¹ The importance of metal-support interactions on catalyst structure and reactivity has been widely recognized,² especially for multi-functional catalysts where the catalyst and its support are active.³ Charge transfer, adsorbate spillover, surface reconstruction, and oxide encapsulation are manifestations of metal-support interactions.⁴⁻⁷ Metal-support interfacial sites are often implicated in catalytic reactions, such as CO oxidation, water gas shift, biomass hydrodeoxygenation (HDO), and CO₂ hydrogenation to methanol.⁸⁻¹² Advancements in catalyst synthesis and characterization have provided valuable atomic-scale insights into the working mechanisms of these catalysts.¹³

 γ -Al₂O₃-supported Pt clusters and nanoparticles are popular supported metal catalysts active for a diverse range of reactions. ¹⁴⁻¹⁶ The sub-coordinated surface Al sites on γ -Al₂O₃ can disperse Pt clusters and facilitate acid-base reactions. ¹⁷⁻²⁰ In this vein, the non-oxidative dehydrogenation of alkanes over Pt/ γ -Al₂O₃ reveals several facets of its catalytic nature. Although Pt is the more active phase for this reaction, the γ -Al₂O₃ support has also been shown to exhibit some reactivity, as the high temperature (T > 550 °C) and water-free reaction environment exposes many coordinatively unsaturated surface Al and O sites ("defect" sites) which facilitate the reaction. ²¹ The reaction over these non-reducible sites occurs through a Lewis acid-base mechanism, which has been proposed to initiate by either the heterolytic cleavage of a single C-H bond over an unsaturated Al/O pair or by the simultaneous breaking of two C-H bonds over the pair. ²⁰⁻²² On the other hand, the reaction over Pt clusters initiates through an oxidative addition step, where the C-H bond is broken atop a single Pt atom. ¹⁵ These diverse interactions between an alkane and Pt/ γ -Al₂O₃ demonstrate the complex catalytic properties of even a simple supported metal catalyst.

Beyond considering each active site type in isolation, the interface between a metal species and an alumina surface has also been shown to be active. For instance, the Au/Al₂O₃ interface has been reported to be active for the water gas shift reaction and the Ni/ γ -Al₂O₃ interface for the dissociation of CO₂ in the dry reforming of methane. In previous work, we demonstrated that interactions between Pt₁₀ clusters and dehydroxylated γ -Al₂O₃(110) facilitate hydrogen spillover from Pt to the alumina sites and dynamically restructure the support. We hypothesize that the Lewis acidity of the reconstructed Pt/ γ -Al₂O₃(110) interface differs from that of the virgin γ -Al₂O₃(110) surface. In the interface differs from that of the virgin γ -Al₂O₃(110) surface.

Here, we investigate the role of Pt_{10} clusters and surface reconstruction on the interfacial acidity of Pt_{10}/γ -Al₂O₃(110) using pyridine adsorption on Al sites and H₂ dissociation over Al/O pairs as probes. Pt_{10} clusters and their induced surface reconstructions generally weaken pyridine adsorption in the monodentate Al-N configuration, lowering the Lewis acidity of interfacial Al sites. Yet, metal-Lewis acid

pairs often allow for stronger bound, multidentate Al-N/Pt-C adsorption configurations with very different vibrational signatures of pyridine. Further, surface reconstruction renders some interfacial Al/O acid-base pairs highly reactive for H₂ dissociation. To better understand these measures of Lewis acidity, we constructed and analyzed correlations for the barrier of H₂ dissociation. Monodentate pyridine adsorption only moderately correlates with the stability of the transition state (TS) of H₂ dissociation because a single Al site can participate in multiple H₂ dissociation channels. Unlike conventional geometry-specific scaling relations, we introduce site-specific TS scaling (TSS) relations and show that these are controlled by underlying chemical similarity within distinct TS groups. We demonstrate TS similarity by geometry, distortion/interaction, and electronic structure analyses. Ultimately, we reason that the influence of the Pt₁₀ cluster on the acid-base reactivity of its support can be understood as perturbations to existing reaction channels on the support.

2. Methods

2.1 Structural models

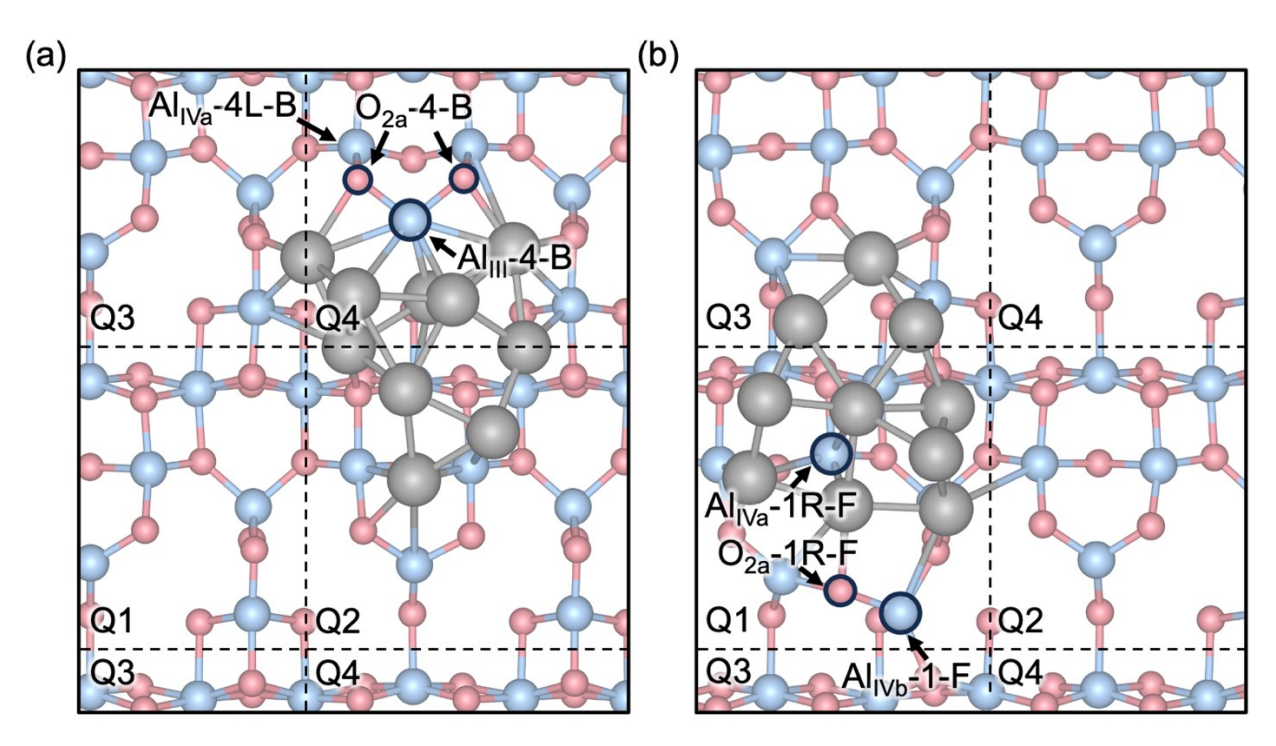


Figure 1. The structure of two Pt₁₀ **clusters of this work.** (a) Geometry of a bilayer Pt₁₀ cluster (sites tagged "-B"). (b) Geometry of a flattened bilayer Pt₁₀ cluster (sites tagged "-F"). The geometries present two of many types of surface reconstructions at the dehydroxylated Pt₁₀/ γ -Al₂O₃(110) interface, one where Pt₁₀-B inserts between Al_{III} and a subsurface O (panel a) and another where Pt₁₀-F inserts between Al_{IVa} and O_{2a} (panel b). Al and O sites around the two clusters are enumerated by quadrant. The periodic image of the 3rd and 4th quadrants is below the 1st and 2nd quadrants.

In this section, we introduce the supported Pt_{10}/γ - $Al_2O_3(110)$ geometries considered in this work; these geometries have been presented previously (**Figure 1**).^{7, 24} Motivated by the activity of Pt/γ - Al_2O_3 for the non-oxidative dehydrogenation of alkanes, we have previously studied the geometry and stability of Pt clusters of varying size, the dependence of reactivity on cluster size, the timescales of selected elementary processes, and the electronic structure of the interface.^{7, 15, 24, 25} We selected a dehydroxylated 8-layer (2×2) cell of γ - $Al_2O_3(110)$, constructed from the non-spinel γ - Al_2O_3 bulk cell, as the support for bare Pt_{10} clusters.²⁶ The Pt_{10} cluster geometries considered here were previously optimized using a basin hopping algorithm, where the potential energy surface of the Pt/γ - $Al_2O_3(110)$ system was represented by a moment tensor potential fitted to density functional theory (DFT) calculations.⁷ Our choice of the alumina surface and Pt cluster structures was motivated by the low chemical potential of H_2O and H_2 under typical kinetics-controlled non-oxidative alkane dehydrogenation reaction environments (T > 550 °C and $P_{H2} \sim 10^{-4}$ bar or lower without co-fed H_2O or oxidants).^{15, 21} These environments correspond to a dehydroxylated γ - $Al_2O_3(110)$ surface and bare Pt clusters.²⁷⁻²⁹

The first Pt_{10} cluster considered is a triangular bilayer one (hereafter denoted as Pt_{10} -B), consisting of 7 Pt atoms in the 1^{st} layer and 3 in the 2^{nd} layer (**Figure 1a**). Pt_{10} -B is inserted between Al_{III} -4-B and a subsurface O (surface Al and O sites are enumerated by quadrant); consequently, O_{2b} -4-B is lifted atop Al_{IVa} -4-B, shifting the surrounding Al_{IVa} -O bonds. Compared to Pt_{10} -B, the second Pt_{10} cluster is flatter and pentagonal (Pt_{10} -F), with 9 Pt atoms in the 1^{st} layer and 1 in the 2^{nd} layer (**Figure 1b**). Unlike Pt_{10} -B, Pt_{10} -F is inserted between Al_{IVa} -1R-F and O_{2a} -1R-F. Al_{IVb} -1-F now bonds with the shifted O_{2a} -1R-F, breaking away from a subsurface O to its right. Beyond these explicit reconstructions, many Al-O bonds surrounding the interface are strained due to bonding with Pt_{10} and surface reconstruction. As surface and interfacial strain are known to impact adsorption energies, calculations survey all Al sites surrounding the two clusters. Al_{IVa} -1

2.2 Density functional theory (DFT) calculations

DFT calculations were performed using the Vienna Ab-initio Simulation Package, version 5.4.1.³²⁻³⁴ The exchange-correlation (XC) energy was calculated using the Perdew-Burke-Ernzerhof (PBE) functional.³⁵ The DFT-D3 method with the Becke-Johnson damping function was used to calculate the van der Waals dispersion energy.^{36, 37} The core electrons were described using the projector augmented-wave method, and one electron wavefunctions were expanded using a basis set of plane waves with kinetic energy up to 400 eV.^{38, 39} Spin polarization was used in all calculations. A dipole correction was applied in the z direction for all calculations of surfaces; on the other hand, quadrupole corrections were used in

all calculations of gases. ⁴⁰ In structural optimizations, the Brillouin zone was sampled at the Γ point only. On the other hand, in the electronic density of states (DOS) calculations, the Brillouin zone was sampled using a (3×3×1) mesh. ⁴¹ The projected DOS (PDOS) and crystal orbital Hamilton population (COHP) calculations were performed using the LOBSTER code, version 4.1.0. ⁴²⁻⁴⁷ The electronic structure in each self-consistent field (SCF) cycle was considered converged when the difference in total energy between consecutive SCF steps fell below 10⁻⁶ eV. The top 3 and bottom 3 layers of the 8-layer slab were relaxed during structural optimizations. The atomic positions were considered converged when the Hellmann-Feynman forces on unconstrained atoms fell below 0.02 eV/Å. Structural optimization of TS was performed using the climbing image nudged elastic band (CI-NEB), dimer, and quasi-Newton algorithms. ⁴⁸⁻⁵⁰ The vibrational frequency calculations were performed using the finite difference method with a step size of 0.01 Å. Each TS was verified to have only 1 imaginary frequency.

3. Results

3.1 Pyridine adsorption and H₂ dissociation at interfacial Al sites

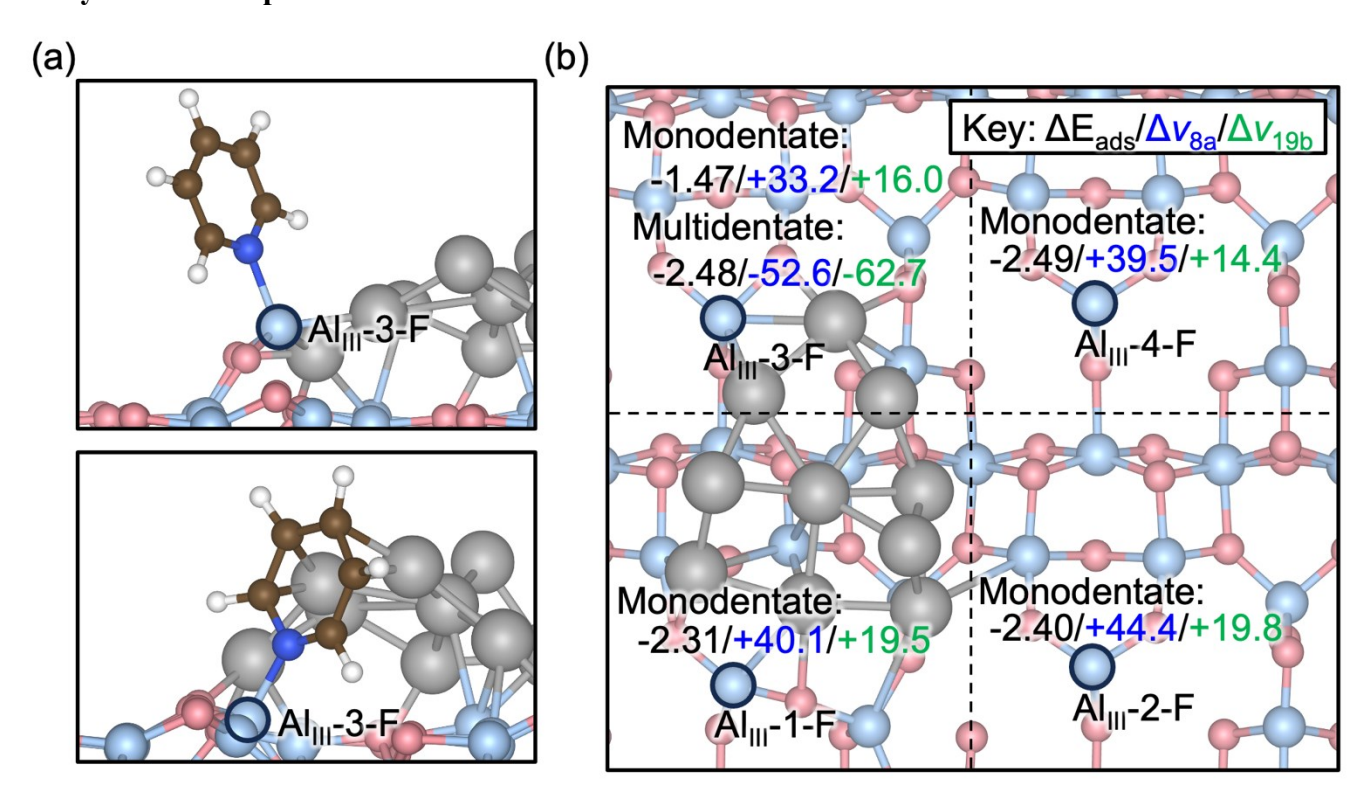


Figure 2. Adsorption of pyridine and its vibrational signatures. (a) Geometry of adsorbed pyridine at the Al_{III}-3-F site near the Pt₁₀-F cluster in a monodentate and a multidentate geometry. (b) Adsorption energy of pyridine ($\Delta E_{ads,pyr}$, units of eV) and shifts in the 8a and 19b vibrational modes (Δv_{8a} and Δv_{19b} , units of cm⁻¹) upon adsorption atop Al_{III} sites near the Pt₁₀-F cluster. When adsorbed in the

monodentate binding mode, $\Delta E_{ads,pyr}$ is weakened on Al sites bound to the Pt cluster. The pyridine 8a vibrational mode appears more sensitive to the adsorption strength than the 19b vibrational mode.

We begin with the adsorption of pyridine at interfacial Al sites near Pt₁₀-F and its vibrational signatures (**Figure 2**). We selected pyridine as the probe molecule because its well-resolved ring vibrational modes allows the user to easily quantify the strength and abundance of acid sites through infrared (IR) spectroscopy. We compare the adsorption energy of pyridine and shifts in its 8a and 19b vibrational modes as a sign of the extrinsic Lewis acidity of Al sites. On the bare γ -Al₂O₃(110) surface, pyridine adsorbs in a monodentate geometry on sub-coordinated Al sites, forming an Al-N bond.⁵¹ Pyridine adsorption at the Al_{III}-3-F, Al_{IVa}-2L-F, and Al_{IVb}-3-F sites is largely weakened, by up to 0.87 eV at Al_{III}-3-F (**Table S1**). At Al sites not bound to Pt, pyridine adsorption could also be weakened if the adsorption site requires further reconstruction, particularly at the Al_{IVa}-4-B sites by 0.54 eV (**Figure S1**). The adsorption on certain Al sites not bound to the Pt cluster is slightly strengthened, particularly Al_{III}-4-F by 0.16 eV. Sites close to the Pt cluster can also adsorb pyridine in a multidentate geometry with C bound to Pt and N bound to Al (**Figure 2a**) and stabilize it sometimes by more than 1 eV compared to the monodentate Al-N configuration at the same site on bare γ -Al₂O₃(110) (**Table S1**).

As the adsorption mode of pyridine controls its vibrational signatures, blueshifts in the 8a and 19b vibrational modes of pyridine are often correlated to surface Lewis acidity.^{52, 53} In the monodentate adsorption mode, a blueshift for both vibrational modes occurs, where the 8a mode is more sensitive to adsorption energy than the 19b mode, in agreement with reported studies (**Table S1**).⁵¹ For instance, comparing pyridine adsorbed at the Al_{III} site of bare alumina to that at the Al_{IVa} site, the 8a mode differs by 7.2 cm⁻¹ but the 19b mode differs by only 3.4 cm⁻¹. All modes experience a severe redshift in multidentate adsorption due to bonding between the aromatic ring and Pt. Overall, our pyridine adsorption survey indicates that Pt's presence generally lowers the acidity of interfacial Al sites. Although most Al sites bound to Pt become less acidic, some remote Al sites not bound to Pt become slightly more acidic, where the adsorption energy of pyridine decreases by ~0.1 eV. The 8a vibrational mode of pyridine is more sensitive than the 19b mode to differences in Lewis acidity.

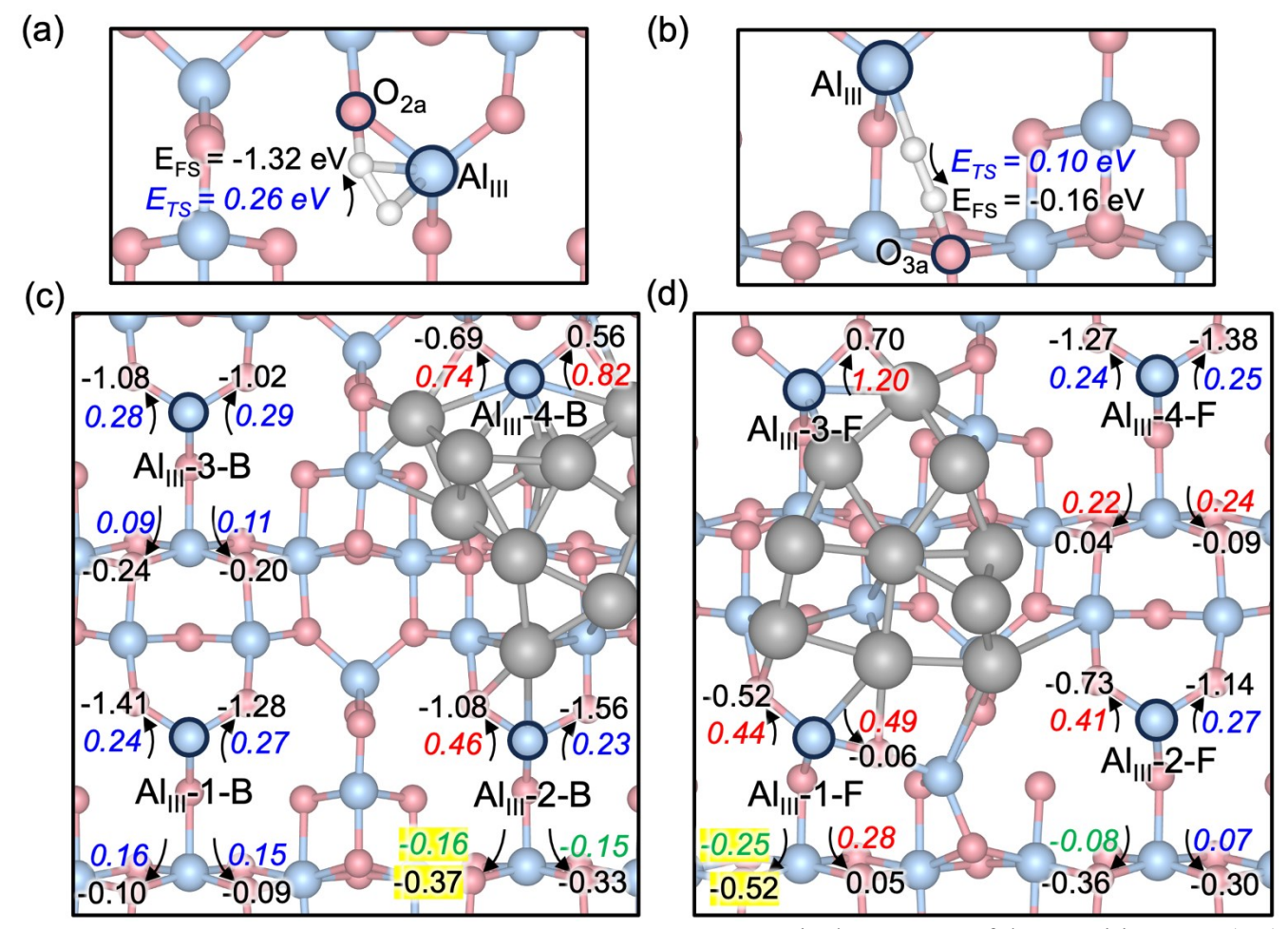


Figure 3. H₂ dissociation energetics over Al_{III}/O pairs. Prototypical geometry of the transition state (TS) of H₂ dissociation over the (a) Al_{III}/O_{2a} and (b) Al_{III}/O_{3a} site pairs on the bare γ-Al₂O₃(110) surface and stability of the TS (E_{TS}) and final state (FS; E_{FS}) relative to H₂ gas. (c) Energetics (units of eV) of the heterolytic dissociation of H₂ over Al_{III}/O pairs near the Pt₁₀-B cluster. (d) Energetics (units of eV) over Al_{III}/O pairs near the Pt₁₀-F cluster. TS stabilized by more than 0.1 eV are labeled green, those destabilized by 0.1 eV are labeled red, and those that did not change by more than 0.1 eV are labeled blue. The most reactive Al/O pair on each surface is highlighted in yellow. Although many Al sites binding to Pt are less active, some Al_{III}/O_{3a} pairs are more reactive due to surface reconstruction.

As a second probe for surface acidity, we computed and compared the energetics of the heterolytic dissociation of H_2 at interfacial Al and O sites (**Figure 3**). We selected H_2 dissociation as it is a simple representative of a larger class of Lewis acid-base elementary reactions, and we compared the dissociation barrier relative to H_2 gas as a sign of Lewis acid-base reactivity.^{18, 20, 54} In our survey, we found little differences in the H_2 dissociation barriers over remote Al_{III}/O_{2a} pairs not bound to the Pt cluster, except over Al_{III} -2-F/ O_{2a} -2L-F, where the TS (E_{TS} ; stability of the TS relative to the bare surface and gaseous H_2) is 0.15 eV less stable compared to that over an Al_{III}/O_{2a} pair on bare γ -Al₂O₃(110). Adjacent Al_{III}/O_{2a} pairs bound to Pt generally become less reactive with a few exceptions. For instance, H_2 dissociation over the adjacent Al_{III} -2-B/ O_{2a} -2R-B pair is more exothermic than H_2 dissociation over the bare γ -Al₂O₃(110)

surface, and E_{TS} is slightly lower (**Figure 3c**). We observed similar trends in the reactivity of adjacent Al/O pairs involving Al_{IVa} and Al_{IVb} (**Table S2**). One exception is Al_{IVa} -3L-F/O_{3a}-3L, where E_{TS} is 0.15 eV more stable compared to that over an Al_{IVa} /O_{3a} pair on bare γ -Al₂O₃(110). These results largely resemble pyridine adsorption, where pyridine's adsorption strength in the monodentate configuration is generally weakened at Pt-bound Al sites but scarcely affected at remote Al sites.

Different from the adjacent Al/O pairs, several non-adjacent Al_{III}/O_{3a} pairs become much more reactive after surface reconstruction (**Figure 3c,d**). In an extreme case over Al_{III}-1-F/O_{3a}-3L-F, the H₂ dissociation barrier only 0.07 eV relative to the weakly bound H₂ precursor, much lower compared to that over an Al_{III}/O_{3a} pair on bare alumina (**Table S2**). Overall, Pt and surface reconstruction appear to have a bilateral effect on the barrier of H₂ dissociation over interfacial Al/O pairs, and some non-adjacent Al/O pairs become highly reactive.

3.2 Predictive correlations for the barrier of H₂ dissociation

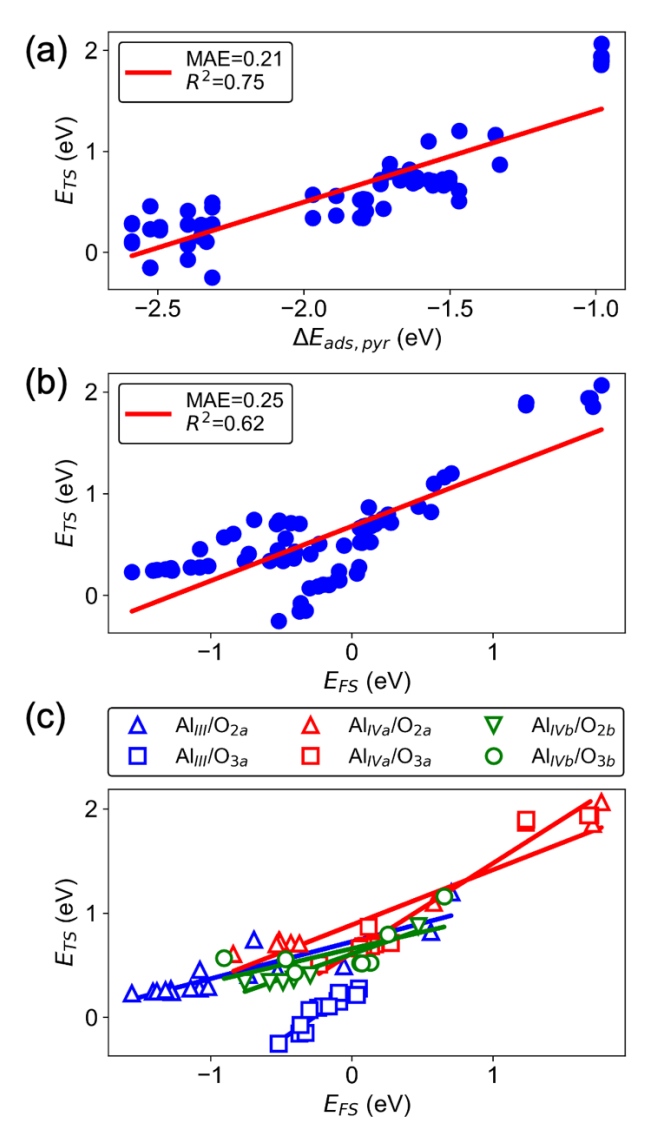


Figure 4. Predictive correlations for the H₂ dissociation barrier. (a) Correlation between the adsorption energy of pyridine in the monodentate configuration ($\Delta E_{ads,pyr}$) and the stability of the TS of H₂ dissociation (E_{TS}), constructed using all datapoints corresponding to both the bare γ-Al₂O₃(110) and the two Pt₁₀/γ-Al₂O₃(110) surfaces. (b) A general final-state scaling (FSS) relation for H₂ dissociation, computed using all datapoints. (c) Site-specific FSS relations for H₂ dissociation. Although a moderate correlation exists between $\Delta E_{ads,pyr}$ and E_{TS} , there is considerable scatter because a single Al site could facilitate multiple reaction pathways. Site-specific TSS relations perform much better than general TSS relations.

As both the adsorption of pyridine and the dissociation of H_2 are linked to the Lewis acidity of interfacial Al sites, the barrier of H_2 dissociation may be correlated with a descriptor. We attempted three such predictive correlations: 1) pyridine adsorption energy at the Al site in the monodentate configuration ($\Delta E_{ads,pyr}$) and E_{TS} , 2) a final-state scaling (FSS) relation, and 3) a Brønsted-Evans-Polanyi (BEP) relation (**Figure 4 and S2**). All datapoints corresponding to both the bare γ -Al₂O₃(110) and the two Pt₁₀/ γ -

 $Al_2O_3(110)$ surfaces are used to construct the correlations. We found $\Delta E_{ads,pyr}$ to be a moderate predictor of E_{TS} , with a coefficient of determination (R²) of 0.75 and a mean absolute error (MAE) of 0.21 eV (**Figure 4a**). The scatter arises from multiple possible reaction pathways involving a single Al site; for instance, the E_{TS} of H₂ dissociation channels over Al_{III}-2-B and Al_{III}-1-F can locally vary by more than 0.6 eV. There is poor single-value correspondence between the two sets of energetics.

At first glance, the general FSS and BEP relations appear to be much worse predictors of the dissociation barrier of H_2 than $\Delta E_{ads,pyr}$ (**Figure 4b and S2a**). For the general FSS and BEP relations, R^2 was 0.62 and 0.55, and MAE was 0.25 and 0.24 eV, respectively. We note the resemblance between the distributions of FSS and BEP datapoints as the initial state of the reaction is a weakly-bound H_2 , whose adsorption energy varies by less than 0.3 eV across Al sites (**Table S2**). Taking a closer look at the distributions, we find a clear stratification: the H_2 reactivity of each Al/O pair scales better with E_{FS} when grouped than a general relation comprising all data, with MAEs reduced to 0.15 eV and below (**Figure 4c and Table S3**). This stratification is especially apparent for the non-adjacent Al_{III}/O_{3a} pairs, all lying below the data corresponding to adjacent Al/O pairs for both the FSS and BEP relations; we suspect that the chemical nature of the dissociation trajectory of H_2 differs at this Al/O pair. On the other hand, the correlation between $\Delta E_{ads,pyr}$ and E_{TS} also improves by adopting site-specific correlations (**Figure S2c**).

Overall, although $\Delta E_{ads,pyr}$ and E_{TS} are generally moderately correlated, the relationship cannot discern differences among the energetics of the multiple possible reaction channels occurring over a single Al site, leading to considerable scatter. On the other hand, site-specific correlations for the H₂ dissociation barrier perform much better.

3.3 Analysis of the TS of H₂ dissociation

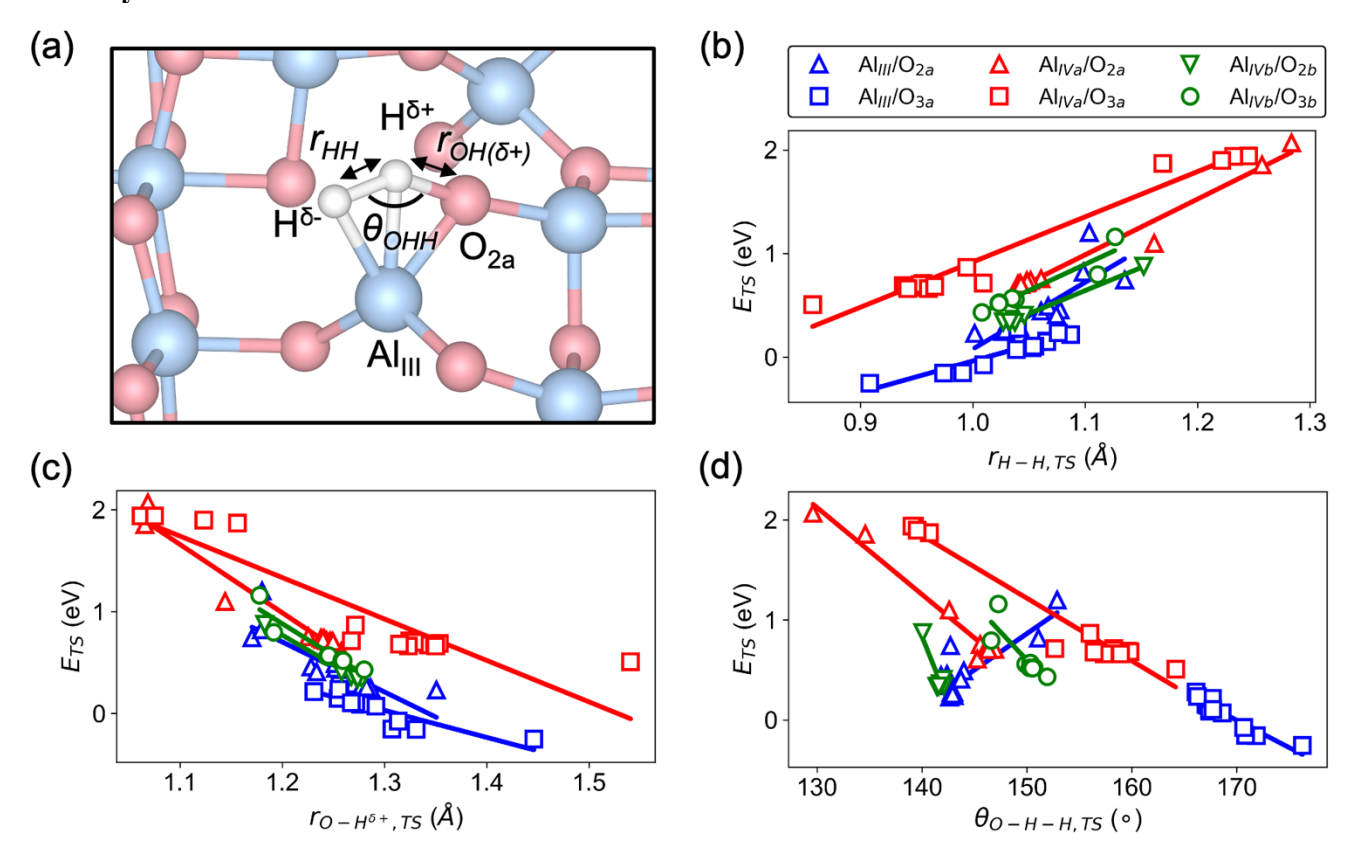


Figure 5. Structural similarities among the TS of H₂ dissociation. (a) Key bond lengths and angles in the TS of H₂ dissociation, as indicated on that over the adjacent Al_{III}/O_{2a} pair. (b) Site-specific correlations between E_{TS} and the H-H bond length. (c) Site-specific correlations between E_{TS} and the O-H-H bond angle. Correlations between E_{TS} and structural characteristics denoted in (a) are site-specific and nearly parallel; outliers in the Al_{III}/O_{2a} correlations are due to the bonding between Al and Pt.

The stratification of H_2 dissociation barrier scaling relations at the Pt_{10}/γ - $Al_2O_3(110)$ interface departs from typical single-descriptor-based scaling relations and warrants a closer inspection. Intuitively, we hypothesize that stratification occurs because each TS group is chemically distinct and responds differently to structural perturbations induced by the Pt_{10} cluster. We performed geometric, energetic, and electronic structural analyses on the H_2 dissociation TS at the bare γ - $Al_2O_3(110)$ surface and the metal-support interface. Like the FSS and BEP relations, we expect stratification in these geometric and energetic signatures.

We begin by comparing the structure of the TS, particularly the bond lengths and angles among the 4 atoms involved in the TS (**Figure 5 and S3**). Like the TSS relations, we observed stratification when correlating E_{TS} and various structural characteristics. Each Al/O pair appears to follow a distinct structural correlation, where E_{TS} is more strongly correlated with the O-H bond length, the H-H bond length, and the O-H-H bond angle (**Figure 5b-d**). Barring a few outliers, these site-specific structural correlations are

remarkably parallel. Recalculating the structural characteristics and E_{TS} as differences relative to those of the TS of H₂ dissociation over the corresponding Al/O pair on bare γ -Al₂O₃(110) results in nearly unified correlations (**Figure S4a-c**). These correlations indicate structural similarity within each TS group and structural difference among TS groups, highlighting their differing underlying chemistry. Crucially, they also demonstrate that these reaction channels at and near the Pt₁₀/ γ -Al₂O₃(110) interface can be treated as structurally perturbed by metal-support interactions compared to those on the bare γ -Al₂O₃(110) surface, confirming our hypothesis.

Despite these important implications of the stratified structural correlations, they cannot individually fully inform the underlying chemistry. For example, the stretching of an H-H bond may happen due to either (or both) charge donation from the occupied H_2 σ orbital or charge donation to the unoccupied H_2 σ^* orbital.⁵⁵ As such, we next seek to group the contributions of these structural qualities through a distortion/interaction analysis and understand the fundamental chemistry through an electronic structural analysis.

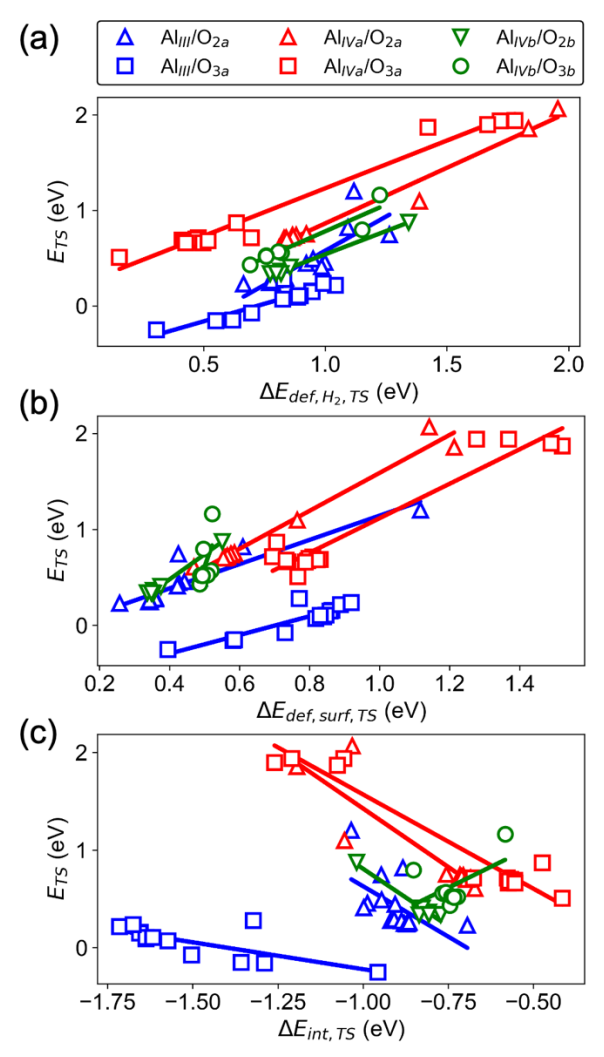


Figure 6. Distortion/interaction analysis of the H₂ dissociation TS. (a) Correlation between E_{TS} and the energy penalty to stretch the H₂ molecule to the TS geometry (E_{def,H_2}). (b) Energy penalty to distort the respective Pt₁₀/ γ -Al₂O₃(110) surface to the TS geometry ($E_{def,surf}$). (c) Interaction energy between the distorted molecule and surface to form the TS geometry (E_{int}). Like with the structural characteristics, correlations between E_{TS} and each energetic component are stratified.

To elucidate the collective contributions of the various structural characteristics, we performed a distortion/interaction (D/I) analysis of the TS of H₂ dissociation (**Figure 6**). We partitioned E_{TS} into three components: E_{def,H_2} as the energy penalty to stretch the H-H bond distance of gaseous H₂ to that in the TS geometry, $E_{def,surf}$ as the energy penalty to distort the Pt₁₀/ γ -Al₂O₃(110) surface to that in the TS geometry, and E_{int} as the interaction energy between the stretched H₂ molecule and the distorted surface ($E_{TS} = E_{def,H_2} + E_{def,surf} + E_{int}$).

Expectedly, E_{TS} and each energy component follow stratified correlations. E_{def,H_2} is fully analogous to the H-H bond distance in the TS and indicates that the longer the H₂ molecule must stretch in its approach to the surface, the less stable the TS. $E_{def,surf}$ represents the required distortions of the

active site structure beyond simply the distance between the Al/O pair involved in the TS, which by itself correlates poorly with the E_{TS} (**Figure S3a and S4d**). $E_{def,surf}$ indicates that the more the active site must distort, the less stable the TS. Finally, E_{int} represents the interaction strength between the stretched H₂ molecule and the distorted active site. E_{int} and the structural characteristics indicate that to stabilize the TS, the interaction between H₂ and the O site should be minimized, which is expressed in a mild preference for H₂ to remain near the Al end of the Al/O pair and the preference for a wider H-H-O angle (**Figure 5 and S3b**). Like the correlations between the structural characteristics and E_{TS} , we expect that the results of the D/I analysis could also be interpreted in terms of deviations from the reference TS structures. Plotting the differences in the energetic contributions from those of the TS on bare γ -Al₂O₃(110), we again find nearly unified correlations, indicating structural similarity within stratified TS groups (**Figure S5**).

Overall, the D/I analysis allows us to combine the individual structural aspects into general qualities of the TS complex. The site-specific correlations between E_{TS} and each energy component indicate that a favorable TS should minimize H_2 and active site distortion and the interaction between H_2 and the O site.

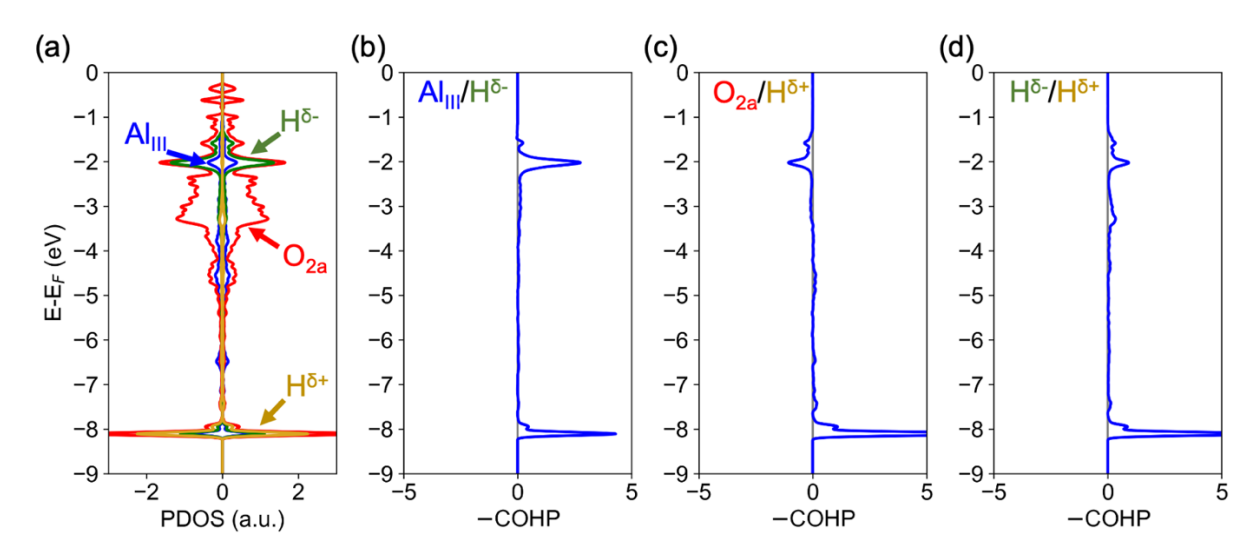


Figure 7. Electronic structure of the TS of H₂ dissociation over Al_{III}/O_{2a}. (a) Projected density of states (PDOS) of the TS of H₂ dissociation over the adjacent Al_{III}/O_{2a} pair of the bare γ-Al₂O₃(110) surface. (b-d) Crystal orbital Hamilton population (COHP) between (b) Al_{III} and H^{δ-}, (c) O_{2a} and H^{δ+}, and (d) H^{δ+} and H^{δ-}.

Although the structural and energetic analyses demonstrate that a favorable H_2 dissociation TS should present an Al-biased structure, and that metal-support interactions can guide existing TS geometries on bare γ -Al₂O₃(110) towards it, it is unclear why such an arrangement is favored. To understand this tendency, we analyze the underlying electronic interactions in the TS of H_2 dissociation

(**Figure 7**). Using the TS of H₂ dissociation over the adjacent Al_{III}/O_{2a} pair of the bare γ -Al₂O₃(110) surface as an example, we first examine PDOS of the TS complex and charge density difference isosurfaces (**Figure S6a**). The PDOS and charge density differences show a strong polarization of the H₂ molecule by the Al_{III}/O_{2a} pair, with interactions between H₂ and the Lewis-basic O_{2a} and the Lewis-acidic Al_{III}. The interaction between H₂ and O explains the negative correlations between E_{TS} and θ_{OHH} , as 3-center 4-electron bonding is often associated with linear geometries. Further quantification by COHP analysis indicates that the interaction between O_{2a} and H^{δ+} contains both bonding and anti-bonding components, while the interaction between H^{δ-} and Al is of purely bonding character. This difference in the interaction modes explains the negative correlations between E_{TS} and $r_{O-H^{\delta+}}$ and Al-biased structural arrangements of favorable TS structures. The purely-bonding interaction between H^{δ-} and Al is also compatible with the moderate positive correlation of E_{TS} and $\Delta E_{ads,pyr}$, as $\Delta E_{ads,pyr}$ is an explicit indicator of Lewis acidity. Similar electronic interactions are found for H₂ dissociation over the non-adjacent Al_{III}/O_{3a} pair (**Figures S6 and S7**). Overall, our electronic structure analysis informs the chemistry underlying the structural and energetic correlations, forming a basis for understanding trends in the stratification of TSS relations.

4. Discussion

4.1 Surface and interfacial acidity of Pt/γ-Al₂O₃ and their role in bifunctional reaction mechanisms

Our data indicates a moderate correlation exists between $\Delta E_{ads,pyr}$ and E_{TS} of H₂ dissociation due to the importance of Al Lewis acidity in stabilizing H₂, but a significant scatter also exists because a single Al site participates in multiple H₂ dissociation pathways. Generally, it has been recognized that the acidity of an active site probed by the adsorption of a basic probe molecule does not necessarily indicate its activity in an elementary acid-base reaction.⁵⁷ In our case, the lack of better correlations underlines the importance of active site structure, as evidenced by the utility of site-specific TSS relations. The roles of O site basicity and Al/O site structure were highlighted when H₂ and CH₄ dissociation barriers over γ -Al₂O₃(110) were compared as a function of OH coverage.¹⁸ Hydroxylation-induced Al site reconstruction, surface O sites' enhanced basicity, and novel reaction channels were reported to lower H₂ and CH₄ dissociation barriers at a low OH coverage (*ca.* 3 OH/nm²) compared to the fully dehydroxylated surface.¹⁸

Although the enhanced reactivity of interfacial Al/O pairs due to metal-support interactions appears exciting, we recognize that our present results are only applicable to harsh reaction environments with a negligible coverage of hydroxyls on γ -Al₂O₃(110). At high (\geq 8.9 OH/nm²) hydroxyl coverages, almost all surface Al sites on γ -Al₂O₃(110) will be blocked, and metal clusters can only interact through the surface hydroxyl groups. ^{58, 59} In this case, Pt clusters will affect the Brønsted acidity of the surface, as

oxidation of the cluster by the reverse spillover of H^+ has been reported. On the other hand, due to the strong adhesion of Pt clusters to surface Al/O sites, smaller Pt clusters (2-3 atoms) have also been reported to displace OH groups on hydrated γ -Al₂O₃(110) by inserting between Al and O.⁶⁰ Beyond the bare Al and O sites considered here, we expect Pt clusters to have a noticeable impact on the Lewis acid/base reactivity of hydroxylated γ -Al₂O₃(110) surfaces as well; though, we anticipate the influence to be far more complex as, alongside Pt clusters, adsorbed water is also known to induce surface Al reconstruction. ^{18, 28}

In general, support acidity has important ramifications for bifunctional reactions catalyzed by Pt/y-Al₂O₃ which invoke acid/base reaction steps on the support or at the interface. Revisiting the non-oxidative dehydrogenation of alkanes over Pt/y-Al₂O₃, the perturbed Lewis acid/base reactivity of interfacial Al/O pairs will influence the background activity due to the support. Here, our scaling relation-based approach can serve as an expediate way to assess the impact of metal-support interactions. In the steam reforming of ethanol over Pt/γ-Al₂O₃, ethanol dehydration to ethylene takes place over Lewis acid sites on the support.⁶¹ Ethylene in the temperature-programmed desorption (TPD) of ethanol started desorbing at a lower temperature on Pt/γ-Al₂O₃ than γ-Al₂O₃ itself, but at a significantly lower concentration because much of the transiently produced ethylene decomposed on the Pt sites.⁶¹ Considering that dispersed Pt clusters can alter the abundance and strength of Lewis acid/base sites on the support, we anticipate that our approach may be extended to develop a multi-site kinetic model which includes metal-support interactions. An enhanced Lewis acid/base reactivity of interfacial sites may ultimately favor a bifunctional mechanism for ethanol reforming. In the HDO of m-cresol over supported Pt/y-Al₂O₃, dehydration of (partially) hydrogenated intermediates by Lewis acid sites on the support was proposed as the C-O bond cleavage step. 14,62 Alloying Pt with Co or Ni improved the reactivity due to enhanced acidity of the γ-Al₂O₃ support from Co or Ni.⁶² We note a similar effect in the product selectivity of polyethylene hydrogenolysis over nickel aluminate catalysts.⁶³ Focusing on Pt, as the influence of Pt clusters on the support surface structure depends on cluster size,^{7, 60} we anticipate that the reactivity of a Pt/γ-Al₂O₃ catalyst for HDO will not only depend on the number of Pt sites but also on the dispersion of the Pt clusters.

Beyond simply considering the Lewis acid/base activity of the support surface, several studies have recognized that the proximity of active support sites and metal sites can activate multidentate adsorbates. For instance, the dissociation of CO₂ is a key step in the dry reforming of methane and the reduction of CO₂. Over γ-Al₂O₃-supported metal catalysts (e.g. Ni and Cu nanoparticles), CO₂ has been shown to dissociate over interfacial metal/Al pairs.^{23,64} On the other hand, Pt/MgO has been shown to be active for the water-gas shift reaction, where the formation of the carboxyl intermediate at the

Pt/MgO(100) interface was identified as the rate-determining step at realistic CO coverages.⁶⁵ These observations are echoed in our present work, as we observed that pyridine can adsorb in a multidentate mode at the Pt/γ -Al₂O₃(110) interface, involving both Pt-C and Al-N interactions. Despite the attractiveness of these interfacial sites, we recognize that they may also compromise selectivity. For instance, the abundance of Lewis acidic tetrahedral Ni^{2+} sites near Ni nanoparticles in nickel aluminate catalysts was found to be positively correlated with the selectivity for methane in polyethylene hydrogenolysis.⁶³

4.2 Characterization of metal/Lewis acid bifunctional catalysts using pyridine

The pyridine adsorption calculations indicate that pyridine adsorption is weaker in the monodentate configuration at Pt-bound Al sites and stronger in the multidentate configuration.²⁴ As metal clusters are known to bind to the Lewis acid sites of γ-Al₂O₃, a naive conceptualization is that a supported metal catalyst should have fewer and weaker Lewis acid sites on the support.^{17, 58, 59} To our knowledge, there is no consensus on how dispersed Pt species influences the abundance of Lewis acid sites on an acidic support, as quantified by pyridine chemisorption.^{66, 67} For Pt/γ-Al₂O₃, surface Lewis-acid sites has been reported to be slightly weaker based on the position of the 8a vibrational mode of adsorbed pyridine (a shift from 1615 cm⁻¹ to 1613 cm⁻¹, much weaker than those found here), but they also has been reported to be more abundant based on the integrated 19b peak area.^{68, 69} Catalyst synthesis and pretreatment procedures influence the acidity; particularly, the acidity of γ-Al₂O₃ is sensitive to residual Na⁺, K⁺, F⁻, and Cl⁻ and the OH coverage.^{14, 18, 70, 71} The importance of metal-acid site balance in bifunctional hydrocracking catalysts necessitates control experiments to guide catalyst design.⁷²

The chemisorption of pyridine on transition metal surfaces differs from the M-N adduct configuration on metal oxides, as indicated by vibrational spectroscopy. At low coverage and low temperature (ca. 100 K), pyridine adsorbs on Pt(110) and Pt(111) flat, similar to the multidentate configuration of our prior work but in an upright monodentate adsorption configuration at high coverage. Here, upright pyridine's vibrational signatures are reminiscent of pyridine adsorbed on Lewis acid sites. Irreversibly bound α -pyridyl species, whose principal ring vibrational modes fall in the same 1200-1700 cm⁻¹ window as pyridine, can be produced by warming the surface to ca. 300 K or by chemisorption at similar temperatures. As such, considerations have been reported to avoid these complications when characterizing conventional catalysts. First, the infrared (IR) spectra of adsorbed pyridine can be assigned to separate pyridine and α -pyridyl peaks. Second, it has been reported that pyridine chemisorption at elevated temperatures (ca. 400 K or above) suffers less from this issue.

4.3 TSS relationships at the metal-support interface and the mechanism of H₂ activation

TSS relations at and near the metal-support interface are stratified and reflect the non-uniform impact of Pt on the acid/base reactivity of the support. Similarities among H-H bond activation, alkane dehydrogenation, and alcohol dehydration over γ -Al₂O₃ have been recognized.^{20, 54} We expect other Lewis-acid/base reactions at and near the metal-support interface to be affected in a site-specific and adsorbate-specific fashion.

As the closest analog to H₂ dissociation, CH₄ dissociation over γ-Al₂O₃ has been extensively compared to H₂ dissociation. ¹⁸ C-H bond activation over oxides and oxygen-precovered metal surfaces entails either a homolytic reaction, whose TS resembles that of the oxygen rebound mechanism, ⁸⁰ or a surface-stabilized heterolytic reaction. ⁸¹ General scaling relations have been reported for both mechanisms. ⁸²⁻⁸⁴ Although deviations from conventional scaling relations have been recognized at the metal-support interface, ^{31,85} the stratified TSS relations here represent a different perspective focusing on local structural deviations. These finer differences resemble the impact of strain on the reactivity of metal surfaces, where each surface and adsorbate respond differently to the same applied strain. ^{30,86} As metal-support interaction and reaction-induced strain on the support have been observed by time-resolved microscopy, ⁸⁷ characterizing and analyzing the multi-timescale kinetics using site-specific scaling relations could be an effective strategy.

Aside from structural perturbations to TS geometries, the stratification of TSS relations is likely also due to the differing mechanisms through which H₂ dissociation proceeds, as we have shown in our structural and energetic analyses. The mechanism of heterolytic H₂ activation has been extensively studied in molecular systems. *d*⁰ transition metal and lanthanide hydrides are known to catalyze the σ-bond metathesis reaction, while main-group frustrated Lewis pairs (FLPs) are known to dissociate H₂.^{88,89} The resemblance between the dissociation of H₂ over the non-adjacent Al_{III}/O_{3a} pair and H₂ activation over main-group FLPs has been recognized, ¹⁸ and similar H₂ dissociation TS geometries have been reported on O-defective CeO₂ surfaces, ZnO, and other systems. ^{89,90} The near-linear H₂-donor configuration in the TS of our calculations agrees with that observed over molecular FLPs and surfaces. ^{55,90,91} The Al-biased structural arrangement in our analyses resembles that reported in mechanistic investigations of H₂ activation by molecular FLPs, where the most feasible H₂ activation TS geometries favor the Lewis-acidic acceptor while attempting to minimize interactions between H₂ and the donor. ⁵⁵ Overall, these structural and chemical influences which result in TSS stratification reflect the diverse chemistry of metal-support interfaces.

5. Conclusions

We studied the influence of Pt clusters on the Lewis acidity of dehydroxylated γ -Al₂O₃(110) through first principles calculations. The bonding between Pt₁₀ and γ -Al₂O₃(110) and subsequent surface reconstruction generally weaken the monodentate pyridine adsorption mode at the interfacial sites but create a stronger multidentate pyridine adsorption mode with very different vibrational signatures. Even though the heterolytic dissociation of H₂ is a Lewis acid-catalyzed reaction, the correlation between the monodentate pyridine adsorption energy and the H₂ dissociation barrier shows considerable scatter. This scatter stems from each Al participating in multiple H₂ dissociation channels and being affected differently by metal-support interactions. Instead, site-specific TSS relations outperform the general scaling relations. Geometric, energetic, and electronic structural analyses reveal the chemical distinctness of the reaction pathways. The stratified structural and energetic correlations and TSS relations suggest that the influence of a dispersed metal species on Lewis acid/base reactions occurring at and near the metal-support interface can be understood as perturbations to existing reaction channels occurring on the bare support.

6. Supporting Information

SI #1: Additional details of pyridine adsorption energetics and vibrational signatures, H_2 dissociation energetics, and TS analyses.

SI #2: Geometry, total energy, and vibrational frequencies of intermediates and transition states referenced in this work. (zip)

7. Conflicts of Interest

There are no conflicts to declare.

8. Acknowledgements

This work was supported by the National Science Foundation's "Designing Materials to Revolutionize and Engineer our Future" (DMREF) program under Award Number 2323700. This research was also partly supported by the high-performance computing resources of the Information Technologies (IT) at the University of Delaware.

9. References

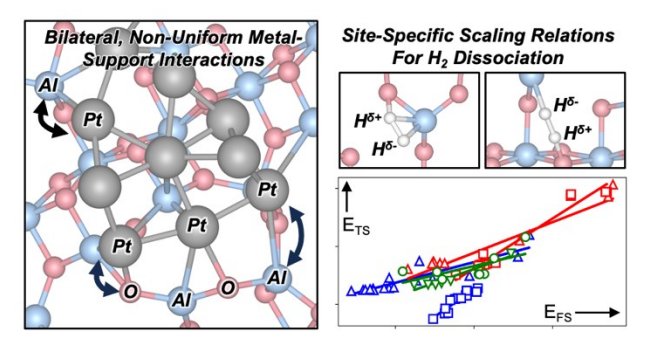
- 1. Liu, L.; Corma, A., Metal catalysts for heterogeneous catalysis: from single atoms to nanoclusters and nanoparticles. *Chem. Rev.* **2018**, *118*, 4981-5079.
- 2. Xu, M.; Peng, M.; Tang, H.; Zhou, W.; Qiao, B.; Ma, D., Renaissance of Strong Metal–Support Interactions. *J. Am. Chem. Soc.* **2024**, *146*, 2290-2307.
- 3. Kumar, G.; Nikolla, E.; Linic, S.; Medlin, J. W.; Janik, M. J., Multicomponent Catalysts: Limitations and Prospects. *ACS Catal.* **2018**, *8*, 3202-3208.
- 4. Lykhach, Y.; Kozlov, S. M.; Skála, T.; Tovt, A.; Stetsovych, V.; Tsud, N.; Dvořák, F.; Johánek, V.; Neitzel, A.; Mysliveček, J., Counting electrons on supported nanoparticles. *Nat. Mater.* **2016**, *15*, 284-288.
- 5. Konda, S. S. M.; Caratzoulas, S.; Vlachos, D. G., Computational Insights into the Role of Metal and Acid Sites in Bifunctional Metal/Zeolite Catalysts: A Case Study of Acetone Hydrogenation to 2-Propanol and Subsequent Dehydration to Propene. *ACS Catal.* **2016**, *6*, 123-133.
- 6. Frey, H.; Beck, A.; Huang, X.; van Bokhoven, J. A.; Willinger, M. G., Dynamic interplay between metal nanoparticles and oxide support under redox conditions. *Science* **2022**, *376*, 982-987.
- 7. Khan, S. A.; Caratzoulas, S.; Vlachos, D. G., Catalyst Cluster-Induced Support Restructuring. *J. Phys. Chem. C* **2023**, *127*, 22277-22286.
- 8. Green, I. X.; Tang, W.; Neurock, M.; Yates, J. T., Jr., Insights into Catalytic Oxidation at the Au/TiO2 Dual Perimeter Sites. *Acc. Chem. Res.* **2014**, *47*, 805-815.
- 9. Saavedra, J.; Doan, H. A.; Pursell, C. J.; Grabow, L. C.; Chandler, B. D., The critical role of water at the gold-titania interface in catalytic CO oxidation. *Science* **2014**, *345*, 1599-1602.
- 10. Shekhar, M.; Wang, J.; Lee, W.-S.; Williams, W. D.; Kim, S. M.; Stach, E. A.; Miller, J. T.; Delgass, W. N.; Ribeiro, F. H., Size and Support Effects for the Water—Gas Shift Catalysis over Gold Nanoparticles Supported on Model Al2O3 and TiO2. *J. Am. Chem. Soc.* **2012**, *134*, 4700-4708.
- 11. Nelson, R. C.; Baek, B.; Ruiz, P.; Goundie, B.; Brooks, A.; Wheeler, M. C.; Frederick, B. G.; Grabow, L. C.; Austin, R. N., Experimental and Theoretical Insights into the Hydrogen-Efficient Direct Hydrodeoxygenation Mechanism of Phenol over Ru/TiO2. *ACS Catal.* **2015**, *5*, 6509-6523.
- 12. Kattel, S.; Ramírez, P. J.; Chen, J. G.; Rodriguez, J. A.; Liu, P., Active sites for CO₂hydrogenation to methanol on Cu/ZnO catalysts. *Science* **2017**, *355*, 1296-1299.
- 13. Liu, J.; Chen, L.; Liu, X., Deep Insight into Characterizing the Metal-Support Interface in Heterogeneous Catalysis. *ACS Catal.* **2024**, *14*, 1987-2002.
- 14. Foster, A. J.; Do, P. T. M.; Lobo, R. F., The Synergy of the Support Acid Function and the Metal Function in the Catalytic Hydrodeoxygenation of m-Cresol. *Top. Catal.* **2012**, *55*, 118-128.
- 15. Liu, Y.; Zong, X.; Patra, A.; Caratzoulas, S.; Vlachos, D. G., Propane Dehydrogenation on PtxSny $(x, y \le 4)$ Clusters on Al2O3(110). *ACS Catal.* **2023**, *13*, 2802-2812.
- 16. Zhang, F.; Zeng, M.; Yappert, R. D.; Sun, J.; Lee, Y.-H.; LaPointe, A. M.; Peters, B.; Abu-Omar, M. M.; Scott, S. L., Polyethylene upcycling to long-chain alkylaromatics by tandem hydrogenolysis/aromatization. *Science* **2020**, *370*, 437-441.
- 17. Kwak, J. H.; Hu, J.; Mei, D.; Yi, C.-W.; Kim, D. H.; Peden, C. H. F.; Allard, L. F.; Szanyi, J., Coordinatively Unsaturated Al3+ Centers as Binding Sites for Active Catalyst Phases of Platinum on gamma-Al2O3. *Science* **2009**, *325*, 1670-1673.
- 18. Wischert, R.; Laurent, P.; Copéret, C.; Delbecq, F.; Sautet, P., γ-Alumina: The Essential and Unexpected Role of Water for the Structure, Stability, and Reactivity of "Defect" Sites. *J. Am. Chem. Soc.* **2012**, *134*, 14430-14449.
- 19. Jenness, G. R.; Christiansen, M. A.; Caratzoulas, S.; Vlachos, D. G.; Gorte, R. J., Site-Dependent Lewis Acidity of γ-Al2O3 and Its Impact on Ethanol Dehydration and Etherification. *J. Phys. Chem. C* **2014**, *118*, 12899-12907.

- 20. Dixit, M.; Kostetskyy, P.; Mpourmpakis, G., Structure–Activity Relationships in Alkane Dehydrogenation on γ-Al2O3: Site-Dependent Reactions. *ACS Catal.* **2018**, *8*, 11570-11578.
- 21. Batchu, S. P.; Wang, H.-L.; Chen, W.; Zheng, W.; Caratzoulas, S.; Lobo, R. F.; Vlachos, D. G., Ethane Dehydrogenation on Single and Dual Centers of Ga-modified γ-Al2O3. *ACS Catal.* **2021**, *11*, 1380-1391.
- 22. Abdelgaid, M.; Dean, J.; Mpourmpakis, G., Improving alkane dehydrogenation activity on γ-Al2O3 through Ga doping. *Catal. Sci. & Technol.* **2020**, *10*, 7194-7202.
- 23. Foppa, L.; Margossian, T.; Kim, S. M.; Müller, C.; Copéret, C.; Larmier, K.; Comas-Vives, A., Contrasting the Role of Ni/Al2O3 Interfaces in Water–Gas Shift and Dry Reforming of Methane. *J. Am. Chem. Soc.* **2017**, *139*, 17128-17139.
- 24. Yan, G.; Khan, S. A.; Vlachos, D. G., Charge Transfer Drives Hydrogen Adsorption, Spillover, and Hydroxylation at the Pt/γ-Al2O3 Interface. *ACS Catal.* **2024**, *14*, 13579-13590.
- 25. Yan, G.; Vlachos, D. G., Unraveling Multiscale Kinetics over Subnanometer Cluster Catalysts: H2 Desorption from Pt3(-H)2/γ-Al2O3(110). *ACS Catal.* **2023**, *13*, 10602-10614.
- 26. Digne, M.; Sautet, P.; Raybaud, P.; Euzen, P.; Toulhoat, H., Use of DFT to achieve a rational understanding of acid–basic properties of γ-alumina surfaces. *J. Catal.* **2004**, *226*, 54-68.
- 27. Gorczyca, A.; Moizan, V.; Chizallet, C.; Proux, O.; Del Net, W.; Lahera, E.; Hazemann, J.-L.; Raybaud, P.; Joly, Y., Monitoring Morphology and Hydrogen Coverage of Nanometric Pt/γ-Al2O3 Particles by In Situ HERFD–XANES and Quantum Simulations. *Angew. Chem. Int. Ed.* **2014**, *53*, 12426-12429.
- 28. Pigeon, T.; Chizallet, C.; Raybaud, P., Revisiting γ -alumina surface models through the topotactic transformation of boehmite surfaces. *J. Catal.* **2022**, *405*, 140-151.
- 29. Vottero, E.; Carosso, M.; Ricchebuono, A.; Jiménez-Ruiz, M.; Pellegrini, R.; Chizallet, C.; Raybaud, P.; Groppo, E.; Piovano, A., Evidence for H2-Induced Ductility in a Pt/Al2O3 Catalyst. *ACS Catal.* **2022**, *12*, 5979-5989.
- 30. Mavrikakis, M.; Hammer, B.; Nørskov, J. K., Effect of Strain on the Reactivity of Metal Surfaces. *Phys. Rev. Lett.* **1998**, *81*, 2819-2822.
- 31. Mehta, P.; Greeley, J.; Delgass, W. N.; Schneider, W. F., Adsorption Energy Correlations at the Metal–Support Boundary. *ACS Catal.* **2017,** *7*, 4707-4715.
- 32. Kresse, G.; Hafner, J., Ab initio molecular dynamics for liquid metals. *Phys. Rev. B* **1993**, *47*, 558-561.
- 33. Kresse, G.; Furthmüller, J., Efficient iterative schemes for ab initio total-energy calculations using a plane-wave basis set. *Phys. Rev. B* **1996,** *54*, 11169-11186.
- 34. Kresse, G.; Furthmüller, J., Efficiency of ab-initio total energy calculations for metals and semiconductors using a plane-wave basis set. *Comput. Mater. Sci.* **1996,** *6*, 15-50.
- 35. Perdew, J. P.; Burke, K.; Ernzerhof, M., Generalized gradient approximation made simple. *Phys. Rev. Lett.* **1996,** 77, 3865-3868.
- 36. Grimme, S.; Antony, J.; Ehrlich, S.; Krieg, H., A consistent and accurate ab initio parametrization of density functional dispersion correction (DFT-D) for the 94 elements H-Pu. *J. Chem. Phys.* **2010**, *132*, 154104.
- 37. Grimme, S.; Ehrlich, S.; Goerigk, L., Effect of the damping function in dispersion corrected density functional theory. *J. Comput. Chem.* **2011**, *32*, 1456-1465.
- 38. Blöchl, P. E., Projector augmented-wave method. *Phys. Rev. B* **1994**, *50*, 17953-17979.
- 39. Kresse, G.; Joubert, D., From ultrasoft pseudopotentials to the projector augmented-wave method. *Phys. Rev. B* **1999**, *59*, 1758-1775.
- 40. Neugebauer, J.; Scheffler, M., Adsorbate-substrate and adsorbate-adsorbate interactions of Na and K adlayers on Al(111). *Phys. Rev. B* **1992**, *46*, 16067-16080.
- 41. Monkhorst, H. J.; Pack, J. D., Special points for Brillouin-zone integrations. *Phys. Rev. B* **1976**, *13*, 5188-5192.

- 42. Dronskowski, R.; Bloechl, P. E., Crystal orbital Hamilton populations (COHP): energy-resolved visualization of chemical bonding in solids based on density-functional calculations. *J. Phys. Chem.* **1993**, 97, 8617-8624.
- 43. Deringer, V. L.; Tchougréeff, A. L.; Dronskowski, R., Crystal Orbital Hamilton Population (COHP) Analysis As Projected from Plane-Wave Basis Sets. *J. Phys. Chem. A* **2011**, *115*, 5461-5466.
- 44. Maintz, S.; Deringer, V. L.; Tchougréeff, A. L.; Dronskowski, R., Analytic projection from planewave and PAW wavefunctions and application to chemical-bonding analysis in solids. *J. Comput. Chem.* **2013**, *34*, 2557-2567.
- 45. Maintz, S.; Deringer, V. L.; Tchougréeff, A. L.; Dronskowski, R., LOBSTER: A tool to extract chemical bonding from plane-wave based DFT. *J. Comput. Chem.* **2016**, *37*, 1030-1035.
- 46. Maintz, S.; Esser, M.; Dronskowski, R., Efficient Rotation of Local Basis Functions Using Real Spherical Harmonics. *Acta Phys. Pol. B* **2016**, *47*, 1165-1175.
- 47. Nelson, R.; Ertural, C.; George, J.; Deringer, V. L.; Hautier, G.; Dronskowski, R., LOBSTER: Local orbital projections, atomic charges, and chemical-bonding analysis from projector-augmented-wave-based density-functional theory. *J. Comput. Chem.* **2020**, *41*, 1931-1940.
- 48. Henkelman, G.; Jónsson, H., A dimer method for finding saddle points on high dimensional potential surfaces using only first derivatives. *J. Chem. Phys.* **1999**, *111*, 7010-7022.
- 49. Henkelman, G.; Jónsson, H., Improved tangent estimate in the nudged elastic band method for finding minimum energy paths and saddle points. *J. Chem. Phys.* **2000**, *113*, 9978-9985.
- 50. Henkelman, G.; Uberuaga, B. P.; Jonsson, H., A climbing image nudged elastic band method for finding saddle points and minimum energy paths. *J. Chem. Phys.* **2000**, *113*, 9901-9904.
- 51. Moroz, I. B.; Larmier, K.; Liao, W.-C.; Copéret, C., Discerning γ-Alumina Surface Sites with Nitrogen-15 Dynamic Nuclear Polarization Surface Enhanced NMR Spectroscopy of Adsorbed Pyridine. *J. Phys. Chem. C* **2018**, *122*, 10871-10882.
- 52. Busca, G., Spectroscopic characterization of the acid properties of metal oxide catalysts. *Catal. Today* **1998**, *41*, 191-206.
- 53. Tamura, M.; Shimizu, K.-i.; Satsuma, A., Comprehensive IR study on acid/base properties of metal oxides. *Appl. Catal. A* **2012**, *433-434*, 135-145.
- 54. Kostetskyy, P.; Nolan, C. M.; Dixit, M.; Mpourmpakis, G., Understanding Alkane Dehydrogenation through Alcohol Dehydration on γ-Al2O3. *Ind. Eng. Chem. Res.* **2018,** *57*, 16657-16663.
- 55. Skara, G.; De Vleeschouwer, F.; Geerlings, P.; De Proft, F.; Pinter, B., Heterolytic Splitting of Molecular Hydrogen by Frustrated and Classical Lewis Pairs: A Unified Reactivity Concept. *Sci. Rep.* **2017**, *7*, 16024.
- 56. Bickelhaupt, F. M.; Houk, K. N., Analyzing Reaction Rates with the Distortion/Interaction-Activation Strain Model. *Angew. Chem. Int. Ed.* **2017**, *56*, 10070-10086.
- 57. Gorte, R. J.; Crossley, S. P., A perspective on catalysis in solid acids. J. Catal. 2019, 375, 524-530.
- 58. Hu, C. H.; Chizallet, C.; Mager-Maury, C.; Corral-Valero, M.; Sautet, P.; Toulhoat, H.; Raybaud, P., Modulation of catalyst particle structure upon support hydroxylation: Ab initio insights into Pd13 and Pt13/γ-Al2O3. *J. Catal.* **2010**, *274*, 99-110.
- 59. Valero, M. C.; Raybaud, P.; Sautet, P., Interplay between molecular adsorption and metal–support interaction for small supported metal clusters: CO and C2H4 adsorption on Pd4/γ-Al2O3. *J. Catal.* **2007**, 247, 339-355.
- 60. Mager-Maury, C.; Chizallet, C.; Sautet, P.; Raybaud, P., Platinum Nanoclusters Stabilized on γ-Alumina by Chlorine Used As a Capping Surface Ligand: A Density Functional Theory Study. *ACS Catal.* **2012**, *2*, 1346-1357.
- 61. Basagiannis, A. C.; Panagiotopoulou, P.; Verykios, X. E., Low Temperature Steam Reforming of Ethanol Over Supported Noble Metal Catalysts. *Top. Catal.* **2008,** *51*, 2-12.

- 62. Do, P. T. M.; Foster, A. J.; Chen, J.; Lobo, R. F., Bimetallic effects in the hydrodeoxygenation of meta-cresol on γ-Al2O3 supported Pt–Ni and Pt–Co catalysts. *Green Chem.* **2012**, *14*, 1388-1397.
- 63. Vance, B. C.; Najmi, S.; Kots, P. A.; Wang, C.; Jeon, S.; Stach, E. A.; Zakharov, D. N.; Marinkovic, N.; Ehrlich, S. N.; Ma, L., et al., Structure–Property Relationships for Nickel Aluminate Catalysts in Polyethylene Hydrogenolysis with Low Methane Selectivity. *JACS Au* **2023**, *3*, 2156-2165.
- 64. Lam, E.; Corral-Pérez, J. J.; Larmier, K.; Noh, G.; Wolf, P.; Comas-Vives, A.; Urakawa, A.; Copéret, C., CO2 Hydrogenation on Cu/Al2O3: Role of the Metal/Support Interface in Driving Activity and Selectivity of a Bifunctional Catalyst. *Angew. Chem. Int. Ed.* **2019**, *58*, 13989-13996.
- 65. Ghanekar, P.; Kubal, J.; Cui, Y.; Mitchell, G.; Delgass, W. N.; Ribeiro, F.; Greeley, J., Catalysis at Metal/Oxide Interfaces: Density Functional Theory and Microkinetic Modeling of Water Gas Shift at Pt/MgO Boundaries. *Top. Catal.* **2020**, *63*, 673-687.
- 66. Kubička, D.; Kumar, N.; Venäläinen, T.; Karhu, H.; Kubičková, I.; Österholm, H.; Murzin, D. Y., Metal—Support Interactions in Zeolite-Supported Noble Metals: Influence of Metal Crystallites on the Support Acidity. *J. Phys. Chem. B* **2006**, *110*, 4937-4946.
- 67. Regali, F.; Liotta, L. F.; Venezia, A. M.; Boutonnet, M.; Järås, S., Hydroconversion of n-hexadecane on Pt/silica-alumina catalysts: Effect of metal loading and support acidity on bifunctional and hydrogenolytic activity. *Appl. Catal. A* **2014**, *469*, 328-339.
- 68. Beard, B. C.; Zhang, Z. C., Probe Molecule Acid-Base Characterization of a Novel Pt/Al2O3 Hydrodechlorination Catalyst. *Catal. Lett.* **2002**, *82*, 1-5.
- 69. Ravenelle, R. M.; Copeland, J. R.; Kim, W.-G.; Crittenden, J. C.; Sievers, C., Structural Changes of γ-Al2O3-Supported Catalysts in Hot Liquid Water. *ACS Catal.* **2011**, *1*, 552-561.
- 70. Roy, S.; Mpourmpakis, G.; Hong, D.-Y.; Vlachos, D. G.; Bhan, A.; Gorte, R. J., Mechanistic Study of Alcohol Dehydration on γ-Al2O3. *ACS Catal.* **2012**, *2*, 1846-1853.
- 71. Digne, M.; Raybaud, P.; Sautet, P.; Guillaume, D.; Toulhoat, H., Atomic Scale Insights on Chlorinated γ-Alumina Surfaces. *J. Am. Chem. Soc.* **2008**, *130*, 11030-11039.
- 72. Weitkamp, J., Catalytic Hydrocracking—Mechanisms and Versatility of the Process. *ChemCatChem* **2012**, *4*, 292-306.
- 73. Grassian, V. H.; Muetterties, E. L., Electron energy loss and thermal desorption spectroscopy of pyridine adsorbed on platinum(111). *J. Phys. Chem.* **1986**, *90*, 5900-5907.
- 74. Surman, M.; Bare, S. R.; Hofmann, P.; King, D. A., The influence of orientation on the H-D exchange reactions in chemisorbed aromatics: Benzene and pyridine adsorbed on Pt{110}. Surf. Sci. 1987, 179, 243-253.
- 75. Haq, S.; King, D. A., Configurational Transitions of Benzene and Pyridine Adsorbed on Pt{111} and Cu{110} Surfaces: An Infrared Study. *J. Phys. Chem.* **1996**, *100*, 16957-16965.
- 76. Kolsbjerg, E. L.; Groves, M. N.; Hammer, B., Pyridine adsorption and diffusion on Pt(111) investigated with density functional theory. *J. Chem. Phys.* **2016**, *144*, 164112.
- 77. Searles, K.; Chan, K. W.; Mendes Burak, J. A.; Zemlyanov, D.; Safonova, O.; Copéret, C., Highly Productive Propane Dehydrogenation Catalyst Using Silica-Supported Ga–Pt Nanoparticles Generated from Single-Sites. *J. Am. Chem. Soc.* **2018**, *140*, 11674-11679.
- 78. Rochlitz, L.; Searles, K.; Alfke, J.; Zemlyanov, D.; Safonova, O. V.; Copéret, C., Silica-supported, narrowly distributed, subnanometric Pt–Zn particles from single sites with high propane dehydrogenation performance. *Chem. Sci.* **2020**, *11*, 1549-1555.
- 79. Stephens, K. J.; Allgeier, A. M.; Bell, A. L.; Carlson, T. R.; Cheng, Y.; Douglas, J. T.; Howe, L. A.; Menning, C. A.; Neuenswander, S. A.; Sengupta, S. K., et al., A Mechanistic Study of Polyol Hydrodeoxygenation over a Bifunctional Pt-WOx/TiO2 Catalyst. *ACS Catal.* **2020**, *10*, 12996-13007.
- 80. Groves, J. T., Key elements of the chemistry of cytochrome P-450: The oxygen rebound mechanism. *J. Chem. Educ.* **1985**, *62*, 928.
- 81. Abdelgaid, M.; Mpourmpakis, G., Structure–Activity Relationships in Lewis Acid–Base Heterogeneous Catalysis. *ACS Catal.* **2022**, *12*, 4268-4289.

- 82. Kumar, G.; Lau, S. L. J.; Krcha, M. D.; Janik, M. J., Correlation of Methane Activation and Oxide Catalyst Reducibility and Its Implications for Oxidative Coupling. *ACS Catal.* **2016**, *6*, 1812-1821.
- 83. Latimer, A. A.; Kulkarni, A. R.; Aljama, H.; Montoya, J. H.; Yoo, J. S.; Tsai, C.; Abild-Pedersen, F.; Studt, F.; Nørskov, J. K., Understanding trends in C–H bond activation in heterogeneous catalysis. *Nat. Mater.* **2017**, *16*, 225-229.
- 84. Latimer, A. A.; Aljama, H.; Kakekhani, A.; Yoo, J. S.; Kulkarni, A.; Tsai, C.; Garcia-Melchor, M.; Abild-Pedersen, F.; Nørskov, J. K., Mechanistic insights into heterogeneous methane activation. *Phys. Chem. Chem. Phys.* **2017**, *19*, 3575-3581.
- 85. Choksi, T.; Majumdar, P.; Greeley, J. P., Electrostatic Origins of Linear Scaling Relationships at Bifunctional Metal/Oxide Interfaces: A Case Study of Au Nanoparticles on Doped MgO Substrates. *Angew. Chem. Int. Ed.* **2018**, *57*, 15410-15414.
- 86. Wittreich, G. R.; Liu, S.; Dauenhauer, P. J.; Vlachos, D. G., Catalytic resonance of ammonia synthesis by simulated dynamic ruthenium crystal strain. *Sci. Adv.* **2022**, *8*, eabl6576.
- 87. Vincent, J. L.; Crozier, P. A., Atomic level fluxional behavior and activity of CeO2-supported Pt catalysts for CO oxidation. *Nat. Commun.* **2021**, *12*, 5789.
- 88. Balcells, D.; Clot, E.; Eisenstein, O., C—H Bond Activation in Transition Metal Species from a Computational Perspective. *Chem. Rev.* **2010**, *110*, 749-823.
- 89. Stephan, D. W., Diverse Uses of the Reaction of Frustrated Lewis Pair (FLP) with Hydrogen. *J. Am. Chem. Soc.* **2021**, *143*, 20002-20014.
- 90. Huang, Z.-Q.; Liu, L.-P.; Qi, S.; Zhang, S.; Qu, Y.; Chang, C.-R., Understanding All-Solid Frustrated-Lewis-Pair Sites on CeO2 from Theoretical Perspectives. *ACS Catal.* **2018**, *8*, 546-554.
- 91. Yu, X.-Y.; Huang, Z.-Q.; Ban, T.; Xu, Y.-H.; Liu, Z.-W.; Chang, C.-R., Finding Natural, Dense, and Stable Frustrated Lewis Pairs on Wurtzite Crystal Surfaces for Small-Molecule Activation. *Angew. Chem. Int. Ed.* **2024**, *63*, e202405405.



TOC Graphic